

## Remote Hyperspectral Imaging of Endolithic Biofilms Using a Robotic Probe

Amanda E. Lowell, Kah-Siew Ho, and Robert A. Lodder\*

Department of Chemistry, A123 Advanced Science and Technology Center, University of Kentucky, Lexington, KY 40506-0286

### ABSTRACT

Many scientists on Earth have concentrated their searches for extraterrestrial life on robotic probes sent to nearby planets and moons. These robotic probes are able to analyze conditions on the planets and transmit data back to Earth. One branch of astrobiology is devoted to duplicating the specified conditions of remote planets and moons on Earth, and identifying the life that survives there under the assumption that similar life might exist elsewhere. Earth analogs for Mars are found in the deserts of Antarctica, and perhaps beneath glaciers, for example. Earth can serve as a useful test bed for robotic probe technology. Cyanobacteria are one of the oldest forms of life on Earth, and similar forms of life may have developed on other planets like Mars as well. NASA has sent several missions to Mars intended to investigate the environment or to search for life, including the Mars Pathfinder / Sojourner mission. While the Pathfinder mission transmitted some of the best data obtained from the Martian surface to date, the long Martian winters and rough terrain limit the amount of data that can be obtained from different locations using a rover that must drive up to a target to sample it. The two Mars Exploration Rovers scheduled to arrive in January 2004 will feature a longer range to search for signs of liquid water. The search for life near locations where water may be intermittently present demands ability to sense life farther from the rover. Hyperspectral imaging can be used to identify astrophysiologically interesting sites from a distance. The rover can then drive up to the site and conduct further sampling. The cyanobacterium *Gloeocapsa* (a blue-green alga) lives in harsh environments where water is intermittently available. *Gloeocapsa* produces mycosporine-like compounds that serve as a UV sunscreen and that can be used as a chemical marker for presence of biofilms. In this study, reflectance measurements

made by a visible - near-IR / IR imager mounted on a battery-powered robot were used to detect the growth of *Gloeocapsa* cyanobacterial colonies on a prepared limestone surface at a distances up to 20 meters.

### INTRODUCTION

Intelligent extraterrestrial life might not transmit signals to other planets, but might instead send robotic probes to explore them. Robots have the potential to detect forms of life that are not intelligent, as well as those that are. As with the human race, it might take too much time and cost too much in resources for the life forms to make the visit themselves. Some even speculate that it might make sense for humans to search for such robotic probes as well as for deliberate beacon signals (Tough, 2002). What would such probes look like? It is difficult to say with certainty, but there is some sense in using our own probes as a starting point. Scrutiny of our robotic technology might suggest some things to look for in other probes (see Fig. 1). Earth's most famous probes are its most recent, like the Mars Pathfinder and Sojourner.

Some researchers believe pools of open water could exist from time to time at the Martian poles (Whitehouse, 2001). They surmise this from the polar images returned by the Viking Orbiter missions in the 1970s and the later Mars Global Surveyor mission. Several locations of possible recent volcano-ice interactions that could result in water pools appear in these images. These images, combined with discoveries made on Earth in which life exists in more extreme environments than had been once thought, suggest that life could now exist in polar regions of Mars where subglacial volcanism has occurred. Close-range studies are planned of the regions to determine whether there are additional indications that water could be present. If water were found on Mars, its locations would be prime candidates for future landers and robots.

\* Author to whom correspondence should be addressed. Email: Lodder@uky.edu

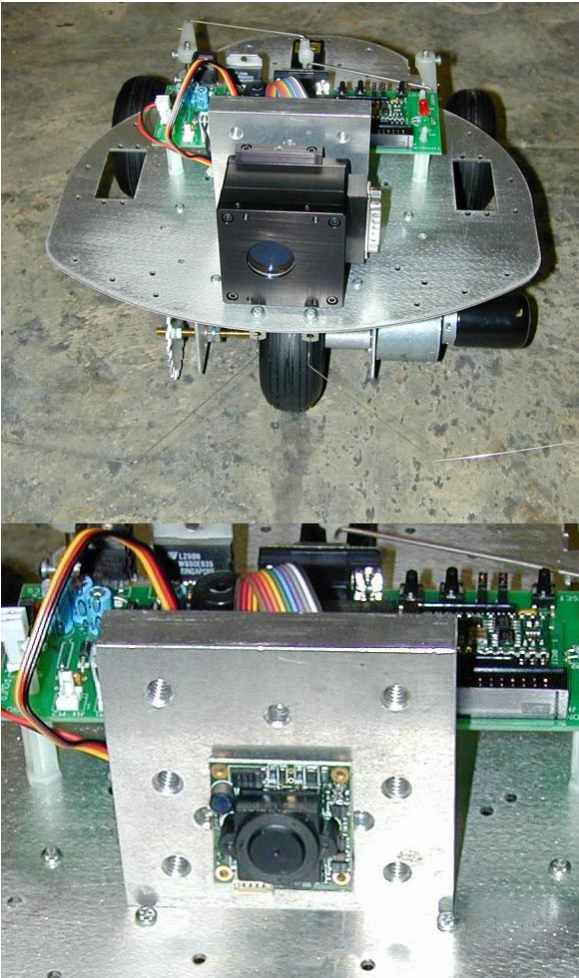


**Fig. 1.** Free roving robot with liquid crystal tunable filter (LCTF) (see top image) installed in front of a CCD camera (see close-up in bottom image) for hyperspectral imaging.

Future robotic missions to Mars are planned to include a vehicle five times larger than Sojourner, the six-wheeled rover on Mars Pathfinder (Race, 1998). This larger robot would have the ability to roam tens of kilometers from its landing vehicle. In contrast, Sojourner traveled only a few meters. The next rover will use a 0.5-cm drill to sample approximately a centimeter into a selection of boulders on the Martian surface. (Boulders can support endolithic biofilms of primitive bacteria as described below). After conducting simple analyses of the composition of each sample and returning the data via telemetry, the rover will transfer the sample to a small container with enough wells to hold ninety-one samples of rock and thirteen samples of soil. The total sample mass should be approximately half a kilogram.

Two years later, according to tentative plans, another rover will fill a similar vault from another part of Mars. Finally, a third lander and rover will arrive to retrieve the samples. In a series of carefully programmed motions, the new rover will retrieve one of the two vaults. The vault selected for retrieval will be the one from whichever site seems have a more interesting set of samples based on the telemetry data from the simple analyses conducted on Mars. The selected vault will be deposited in the third lander. In the planned scheme, the lander will blast off from the Mars but will not return to Earth. To rupture the chain of potential contamination, the lander will rendezvous with a waiting craft in orbit around Mars that never touched the Martian surface. The lander will transfer its cargo, and the orbiting craft will begin its trip back to Earth. Robotic sample-return missions are much more difficult and expensive than in-situ experiments. The complexity and expense of sample return missions argue in favor of supplanting them with in-situ efforts to find life (e.g., hyperspectral imaging endolithic biofilms).

Scientists expect that cyanobacteria (also called blue-green algae) or some form of similar life might exist in the form of endolithic biofilms on Mars. Cyanobacteria are one of the oldest forms of life on Earth, and similar forms of life may have developed on other planets like Mars as well. Cyanobacteria are practically ubiquitous on earth. Species of *Gloeocapsa* form endolithic biofilms on limestone surfaces over much of the U.S., for example. Substantial surface discoloration observed on roofs in the southeast U.S. comes from the cyanobacterium *Gloeocapsa magma*. The spores are carried by the wind from roof to roof. The cells use shingles as a food source. *Gloeocapsa* can feed on the calcium carbonate typically used as a filler material to add weight to shingles. The dark color develops over time as the species attempts to protect itself from sunlight-induced damage. *Gloeocapsa* also forms large communities in areas as diverse as ancient Mayan buildings in Yucatan, Mexico, and as inhospitable as the McMurdo Dry Valley in Antarctica (Banerjee, 2000).

*Gloeocapsa* is common on damp rocks. Spherical cells are typically found in amorphous colonies of >50 cells. The sheath color is variable. Reproduction occurs by cell division and colony fragmentation as described later in the Results and Discussion. *Gloeocapsa sp.* produces mycosporine-like amino acids (MAAs) that serve as UV sunscreens (Garcia, 1993a). Strain C-90-Cal-G accumulates intracellularly an MAA with absorbance maximum at 326 nm, but generates no extracellular sunscreen compound (i.e., scytonemin) (see Fig. 2).

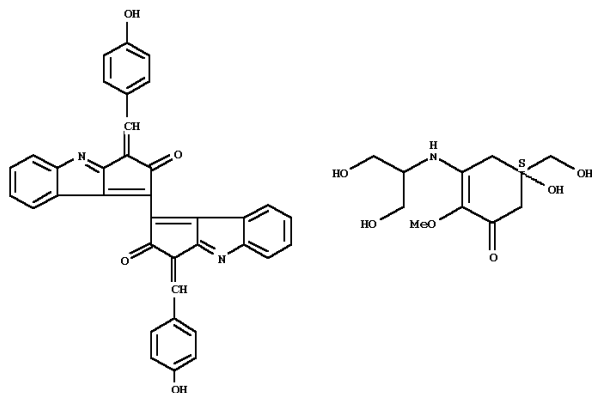


**Fig. 2.** Chemical structures of the UV sunscreen molecules scytonemin (left) and mycosporine, the basis of MAAs (right). Both molecules contain UV and visible as well as near-IR chromophores

The intracellular concentrations of MAA are directly related to the intensity of the UV dose to the cells. A survey of 20 strains of cyanobacteria (belonging to 13 genera) isolated from habitats exposed to bright sunlight showed that 13 strains carried one or more water-soluble, UV-absorbing, MAA-like compounds (Garcia-Pichel, 1993b). Some of the compounds were identical in several strains. A total of 13 distinct MAA compounds were discovered. The UV absorption spectra of MAAs complemented that of the extracellular sunscreen pigment scytonemin, which many of the strains also produced. Under conditions of desiccation, physiological photoprotective and repair mechanisms are inoperative. Colony formation enhances protection by sunscreens and leads to endolithic biofilms readily detected by hyperspectral imaging at great distances.

## EXPERIMENTAL

**Instrumentation.** The basic robot configuration was purchased as a kit (Arobot, Arrick Robotics, Hurst, TX). The model A robot had a large optical platform in the front to accommodate digital cameras and wavelength selection devices. System power (12 VDC) was provided onboard using 8 AA batteries that powered the robot for approximately 5 hours. The robot had only three wheels to enhance stability of the optical platform for imaging applications. A rear wheel provided steering with an RC motor and steering linkage. The rear wheel was not driven, and the front wheels provided the robot's drive. The robot could move at a speed of up to 26 cm/sec, and an optical encoder attached to the front axle reported the robot's speed and position to the onboard computer.

Because the vision was not stereoscopic, the robot navigated at close range using 4 whiskers that covered the zones in which the robot could move (see Fig. 3).

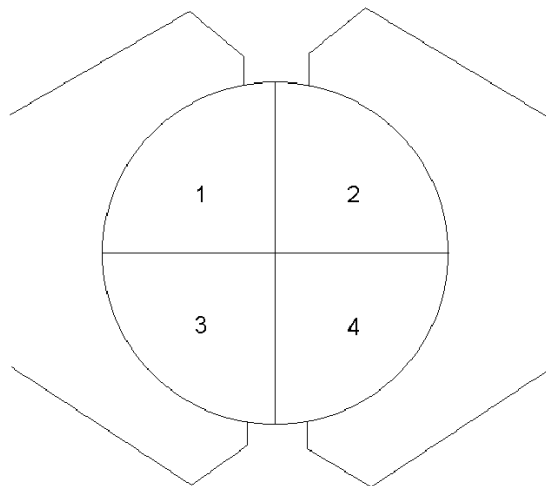


**Fig. 3.** Two pairs of whiskers at the front and rear monitor four zones around the rover.

The robot's onboard computer (Basic Stamp II, Parallax, Rocklin, CA) was designed for controlling locomotion and reading physical contacts via wrap-around whisker sensors. A 2.4 GHz video transmitter and receiver link (RFLink Technology, Torrance, CA) permitted the video digitization and processing to be accomplished remotely. Limitations in the bandwidth of this radio link degrade the spatial resolution of hyperspectral images slightly, however. Because this experiment was intended mainly to demonstrate the ability of spectrometric imaging to detect endolithic biofilms, and because the robot can be operated terrestrially and nearby to accomplish this aim, the video link was not employed. In these experiments, the spectroscopic imaging system was tethered to a notebook computer that could be towed in a passive vehicle by the robot if necessary. Image analysis was accomplished using Mathematica 4.1 (Wolfram Research, Champaign, IL) and Speakeasy IV Eta+ (Speakeasy Computing Corp., Chicago, IL) software.

Spectroscopic imaging in the lower photon energy near-IR band ( $4545\text{-}9090\text{ cm}^{-1}$ ) was accomplished using a filter wheel with ambient

temperature, narrow bandpass filters (10 nm) placed in front of a cold filter (liquid nitrogen cooled) with a broad bandpass (1000 nm). The filters were at 4640, 4810, 5150, 9000  $\text{cm}^{-1}$ . A Si/Ge lens was positioned between the filter systems. An InSb focal plane array near-IR camera (Cincinnati Electronics, Mason, OH) was used to collect the images. The images were digitized and stored in JPEG format using a Macintosh computer (Apple, Cupertino, CA). The low photon energy imaging of biofilms was accomplished at distance of two meters.

Hyperspectral imaging at higher energies (9090-15385  $\text{cm}^{-1}$ ) was accomplished with a liquid crystal tunable filter (CRI, Woburn, MA) and Si CCD (Sharp) camera with zoom lens. Data were collected at 20 different wavenumbers evenly spaced over the spectral range. The camera and filter system operated at ambient temperature. The distance from the biofilm samples to the robot was twenty meters.

The LCTF (see Fig. 4) is an optical filter with no moving parts and a large aperture, large field of view, and good optical quality. The LCTF uses electronically controlled liquid crystal elements to select a transmitted wavelength range, while blocking all others. A single Lyot stage of the LCTF system is a "sandwich" of birefringent liquid crystal, glass, quartz, and sheet polarizers. To achieve monochromatic throughput in the LCTF, a series of these "sandwiches" are stacked horizontally in order of increasing retardance. The bandwidth of the LCTF is constant in frequency space. The filter pass band is electronically tunable over a wide range, and time on the order of milliseconds is required to step through wavelengths or to provide random wavelength access.

Because the filter does not move, there are fewer problems with image registration across many wavelengths. Fig. 5 shows some sample tuning curves for the LCTF in the short-wavelength near-IR region. The optical throughput is highest at the longest wavelengths.

*Samples.* Limestone samples approximately 15x15 cm in size were obtained at a local garden center (Lowes). The wafers served as a substrate to support the endolithic biofilms. The substrates (n=3 for calibration/validation study, and n=1 for interference study) were maintained outdoors throughout the experiment to provide a natural environment for growth of the cyanobacteria. The substrates were inoculated with *Gloeocapsa* (ATCC 29162), placed on an elevated surface (~6 m above ground level), and the cyanobacteria were allowed to grow for 60 days with natural lighting and watering. The wafers were

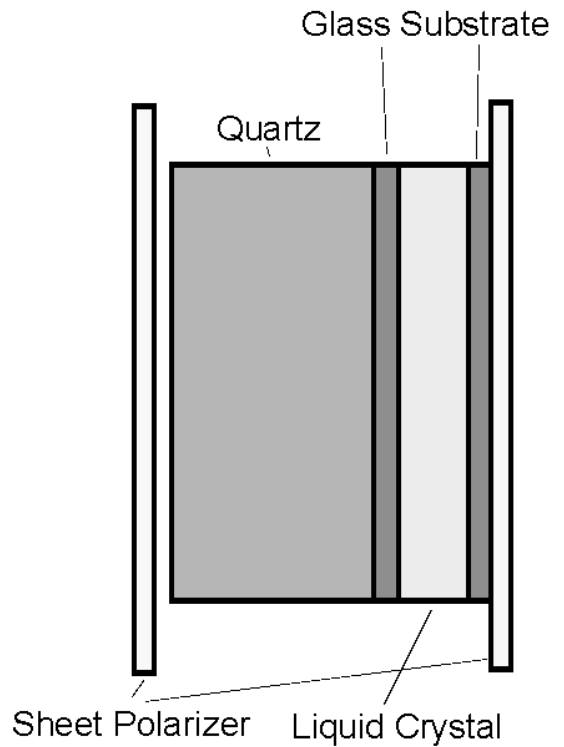


**Fig. 4.** A single Lyot stage of the LCTF system is a "sandwich" of birefringent liquid crystal, glass, quartz, and sheet polarizers. To achieve monochromatic optical throughput in the LCTF, a series of these "sandwiches" are stacked horizontally in order of increasing retardance.

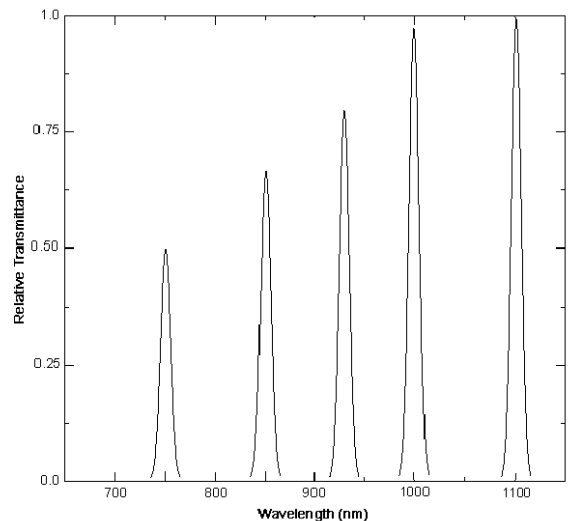


**Fig. 5.** A sampling of tuning curves for the LCTF at different wavelengths shows the bandwidth and tuning range of the filter.

cut down to 5x5 cm for the low energy imaging experiment, while the high energy imaging experiment used the substrates in their original 15x15 cm format. The wafers each served as their own controls because they were imaged before the beginning of the experiment and then were repeatedly imaged over time. Hackberry (*Celtis occidentalis*) pollen for the interference test was harvested from a cylindrical collector mounted horizontally one meter above the ground in a plot of hackberry trees. Collection took place continuously over the months from March to May, with harvesting taking place once at the end of the collection period. Hackberry pollen served a model of indigenous dust in the area where the experiments were performed. The pollen (ca. 10 mg) was added to the wafer at the beginning of the experiment with a camel's hair brush.

**Imaging Chemometrics.** The BEST (Bootstrap Error-adjusted Single-sample Technique) calculates distances in multidimensional asymmetric nonparametric central 68% confidence intervals in spectral hyperspace (approximately equivalent to standard deviations). The BEST metric can be thought of as a "rubber yardstick" with a nail at the center (the multidimensional mean)(Malik, 2001)(Dempsey, 1997). Because of the nail, the stretch of the yardstick in one direction is independent of the stretch in the other direction. This independence enables the BEST metric to describe odd shapes in spectral hyperspace (spectral-point clusters that are not multivariate normal, like the calibration spectra of many biological systems). BEST distances in SDs can be correlated to sample composition to produce a quantitative UV protectant calibration in biofilms, or simply used to identify regions with protectant distributions similar to the calibration data in a spectral image. The BEST automatically detects samples and situations unlike any encountered in the original calibration, making it more accurate in such applications than typical regression approaches to near-IR data analysis. The BEST produces accurate distances even when the number of calibration samples is less than the number of wavelengths used in calibration, in contrast to other metrics that require matrix factorization. The BEST retains the direction vector of a standard deviation in hyperspace throughout all calculations, an essential characteristic for multicomponent quantification of sample composition.

The BEST calculates the integral of a probability "orbital" in hyperspace by starting at the center of the orbital and working outward in all directions at a uniform rate. The distance between the center of a calibration set orbital and a sample spectrum is proportional to the concentration(s) of the calibration set constituent(s) responsible for the vector connecting the central and sample-spectral points. The direction of the vector

identifies the constituent(s) of the calibration set. The BEST direction and distance are often used to create color contour plots of the spatial distribution of UV protectant molecules. In such plots, the contours are drawn at sequential distances in SD's, and RGB (red-green-blue) colors are used to denote class membership based on vector direction. The intensity of the color is proportional to the amount of substance present. Shades of blue are used to represent sample spectra similar to those already in the calibration set, while shades of red are used to represent sample spectra that contain the selected analyte. Shades of green are used to represent a second analyte or possible interfering effect. The BEST performs well as an assimilation method (a method that progressively increases its analytical performance by incorporating previously unknown samples into its calibration). The calibration samples are analyzed by another reference method in the same manner that Beer's Law is used to develop a conventional spectrophotometric calibration.

In the BEST, a population **P** in a hyperspace **R** represents the universe of possible spectrometric samples (the rows of **P** are the individual samples, while the columns are the independent information vectors, such as wavelengths or energies). **P\*** is a discrete realization of **P** based on a calibration set **T**, which has the same dimensions as **P\*** and is chosen only once from **P** to represent as nearly as possible all the variations present in **P**.

**P\*** is calculated using a bootstrap process by an operation  $\kappa(\mathbf{T})$ . To calculate  $\kappa(\mathbf{T})$ , random selections are made with replacement from **T** by filling **P** with the calibration set sample numbers to be used in the bootstrap sample sets **B<sub>(s)</sub>**, and the values in **P** are scaled to the calibration set size *n*:

$$\mathbf{P} = n\mathbf{P} + 1 \quad \text{eq. 1}$$

**P\*** has parameters **B** and **C**, where

$$\mathbf{C} = E(\mathbf{P}) \quad \text{eq. 2}$$

and **B** is the Monte Carlo approximation to the bootstrap distribution. The expectation value,  $E(\ )$ , of **P** is

$$\sigma \left| \frac{\int_0^\sigma \left( \int_{\mathbf{R}} \mathbf{P}^* \rightarrow \vec{CX} \right)}{\int_{\mathbf{R}} \mathbf{P}^* \rightarrow \vec{CX}} \right| = 0.68 \quad \text{eq. 3}$$

the center of  $\mathbf{P}$ , and  $\mathbf{C}$  is a row vector with as many elements as there are columns in  $\mathbf{P}$ .

Each new sample spectrum  $\mathbf{X}$  is analyzed by an operation  $\psi(\mathbf{T}, \mathbf{B}, \mathbf{X}, \mathbf{C})$ , which projects a discrete representation of the probability density of  $\mathbf{P}$  in hyperspace by many-one mapping onto the vector connecting  $\mathbf{C}$  and  $\mathbf{X}$ .  $\mathbf{X}$  and  $\mathbf{C}$  have identical dimensions. The directional standard deviation (SD) is found from the projected probability density in eq 3.

$$C - C_T \rightarrow \vec{CX}$$

eq. 4

The integral over the hyperspace  $\mathbf{R}$  is calculated from the center of  $\mathbf{P}$  outward. The calculation of a skew adjusted is based on a comparison of the expectation value  $\mathbf{C}=E(\mathbf{P})$  and  $\mathbf{C}_T=\text{med}(\mathbf{T})$ , the median of  $\mathbf{T}$  in hyperspace (with the same dimensions as  $\mathbf{C}$ ) projected on the hyperline connecting  $\mathbf{C}$  and  $\mathbf{X}$  in eq 4.

$$+\vec{\sigma} \left| \frac{\int_0^{+\sigma} (\int_{\mathbf{R}} \mathbf{P}^* \rightarrow \vec{CX})}{\int_{\mathbf{R}} \mathbf{P}^* \rightarrow \vec{CX}} \right| = 0.34$$

eq. 5

$$-\vec{\sigma} \left| \frac{\int_0^{-\sigma} (\int_{\mathbf{R}} \mathbf{P}^* \rightarrow \vec{CX})}{\int_{\mathbf{R}} \mathbf{P}^* \rightarrow \vec{CX}} \right| = 0.34$$

eq. 6

The result of the corrected projection is an asymmetric  $\sigma$  that provides two measures of the standard deviation along the hyperline connecting  $\mathbf{C}$  and  $\mathbf{X}$ .

Eq 5 is in the direction of  $\mathbf{X}$  in hyperspace, and eq 6 in the opposite direction along the hyperline connecting  $\mathbf{C}$  and  $\mathbf{X}$ . Skew adjusted SDs can be used to calculate mean distances between spectra of different samples.

The use of these equations in both quantitative and qualitative analysis of samples provides a number of advantages over all other methods of analysis:

1. No analytical assumptions are required to make the problem solvable. Other chemometric methods typically assume that no discriminating variable (wavelength) is a linear combination of other discriminating variables, that the covariance matrices for all spectral groups are approximately equal, and that each group is drawn from a population that is normally distributed on the discriminating variables. None of these assumptions is usually true and violations of these assumptions increase the likelihood of producing incorrect quantitative and qualitative analytical results.

2. This nonparametric assimilation method can be used with full spectra of samples, which often include thousands of variables that describe each sample. The large global memory on the newest supercomputers has made possible the manipulation of images involving millions of spectra at thousands of wavelengths. No wavelength selection procedures or data compression techniques, such as principal-axis transformation or Fourier transformation, are required by this assimilation method in order to analyze complete spectra. Collinearity in the discriminating variables (wavelengths) does not degrade the results. (Collinearity disrupts conventional matrix techniques like the Mahalanobis method, which relies on matrix factorization to produce a distance in SDs.)

3. The vector  $\mathbf{CX}$  in the assimilation method identifies the sample components. The metric is calculated by a highly parallel code that can be distributed across as many processors as are available, and can be used in computerized searches of spectral libraries for qualitative analysis of real samples. The length of the vector is proportional to the concentrations of the constituents. Thus, quantitative analytical capabilities are also provided by the same assimilation method, which can still be distributed across as many processors as are available.

4. The BEST metric is not only more accurate and precise than the Mahalanobis metric (a metric commonly used in near-IR spectrometry), the BEST metric is often calculated more rapidly as well. The matrix inversion required by the Mahalanobis metric is usually accomplished by algorithms whose complexity (in terms of number of operations required) increases as the number of wavelengths cubed. In contrast, the complexity of the BEST metric increases linearly with the number of wavelengths.

The assimilation model developed by the BEST can be compressed if desired with singular value decomposition procedures to conserve memory.

The model can be also be converted into a hash table and hash function after development by calculating the distance and direction from the center of the calibration set to each of the replicates. A new sample spectrum (at one pixel in the hyperspectral image) is determined by looking up the replicate in the direction closest to the new sample, and dividing the Euclidean distance from the center of the replicates to the new sample by the standard deviation stored for that replicate. The number of hyperspectral images desired determines the measured data memory requirement. The hash table typically requires approximately 30 MB of memory. The hash table implementation is several orders of magnitude faster than the model calibration procedure, and can be used in ASIC microchips or laboratory PC's.

## RESULTS AND DISCUSSION

The near-IR spectrum of any sample is composed mainly of overtones and combination bands of fundamental infrared signals. The overtone bands are by nature weaker than the fundamentals ( $< 4000\text{ cm}^{-1}$ ) and far weaker than electronic absorbance bands ( $> 15000\text{ cm}^{-1}$ ). For this reason, the near-IR region offers a working window for light penetration into biological samples whose molecular spectra are otherwise difficult to obtain. The near-infrared spectrum of a *Gloeocapsa* biofilm is shown in Fig. 6.

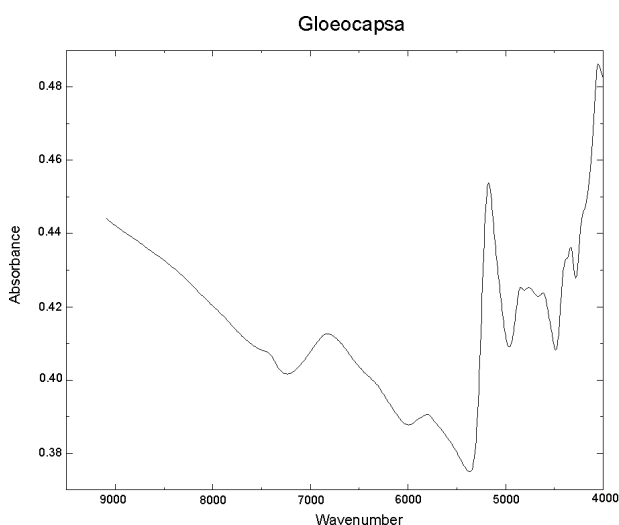


Fig. 6. Near-infrared spectrum of *Gloeocapsa*

The biofilm was sampled directly from a substrate and contains spores and extracellular matrix with scytonemin in addition to cells. This full spectrum was obtained with

a monochromator as a light source to capture all of the peaks in the near-IR region. The absorbance at the higher energy end of the spectrum increases steadily as a result of the intense electronic absorbance of the UV protectant molecules.

The higher energy near-IR imaging experiment used the robot with the LCTF installed as shown in Fig. 1. The larger substrate size was employed because the distance to the samples was greater (20 m vs. 2 m). There are two methods to express the changes monitored by spectrometric imaging in the growing colonies. One method is to depict the size (surface area) covered by a certain density (contour level) of cells, spores, and/or extracellular matrix compounds like UV protectants. This type of display is represented in the contour plots in Fig. 7.

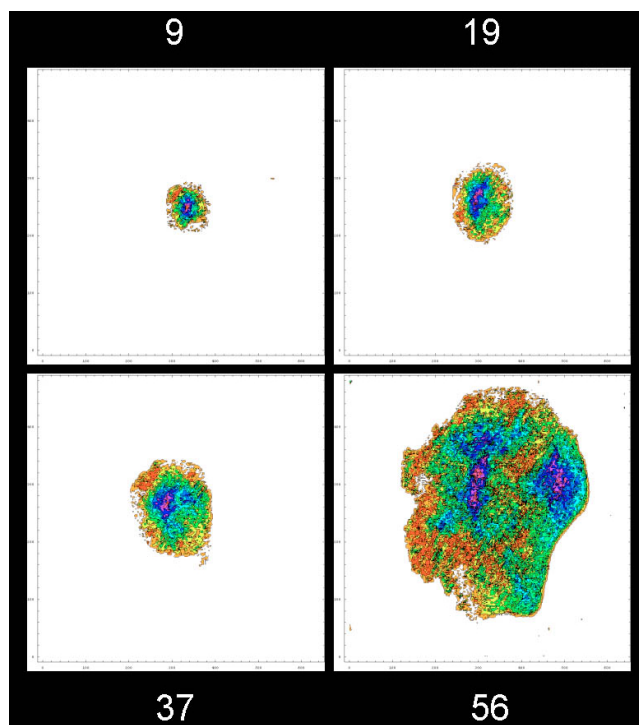
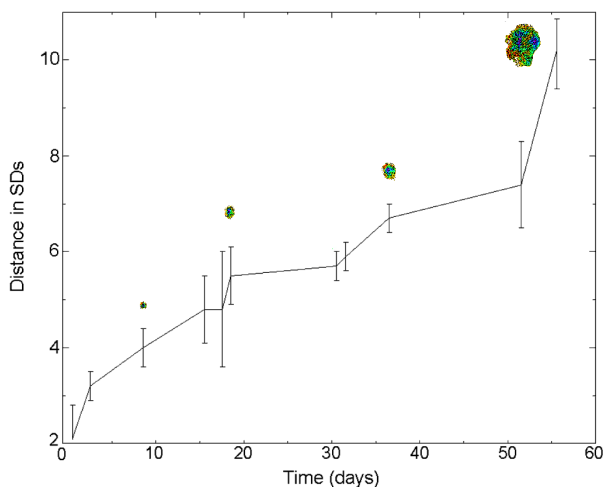


Fig. 7. The BEST contour plots of a *Gloeocapsa* distribution on a 15 x 15-cm limestone wafer in the 9090-15385  $\text{cm}^{-1}$  band at a distance of 20 meters. The 9, 19, 37, and 56 refer to the number of days elapsed since the beginning of the experiment. The x and y axes in the plot represent distance on the surface of the substrate. The z-axis (perpendicular to this page) is the spectrum vector. The contour lines connect pixels with similar spectral vectors. The colony appears to be fragmenting by 56 days.

The most intense signals are depicted in violet and the least intense in red. The other way to express changes is to integrate over all contour levels and surface area covered by cells, spores, and/or extracellular matrix compounds.

The second approach was used to create the line graph in Fig. 8.



**Fig. 8.** The BEST distances (in SDs) integrated over surface area and time (in days) show the growth of a *Gloeocapsa* colony from a distance of two meters using data collected at 4640, 4810, 5150, 9000  $\text{cm}^{-1}$ . The inset contour plots are drawn at the same relative scale to show how the area covered by UV protectant molecules grows with time (9, 19, 37, and 56 days).

The contour plot in Fig. 7 was constructed from four-dimensional data using the Bootstrap Error-adjusted Single-sample Technique (BEST) imaging algorithm (Malik, 2001). The imaging software was calibrated on fresh substrate, and drew the probability density contours connecting pixels with similar spectra 2-9 SDs from the center of the normal, clean substrate. The direction of displacement of the spectral points is controlled by the spectra of the MAAs and scytonemin. Plotting the contours repeatedly over time enables visualization of the colony growth during periods when weather conditions are favorable and water is available.

Using longer wavelength, lower energy photons at a distance of two meters also shows the growth of a *Gloeocapsa* colony in an endolithic biofilm. In Fig. 8, a series of contour plots integrated over surface area and time show how distances of spectra in multidimensional SDs from the fresh substrate increase as the colony grows. The error bars on the mean distances in SDs reflect the standard deviation of the pixels for the entire contoured area. As in Fig. 7, the primary force driving the spectra away over time from the calibration set of fresh substrate spectra is the accumulation of UV protectants (MAAs and scytonemin) in an ever-larger biofilm. Of course, there are more pixels represented in the later-day measurements than in the early ones because the biofilm is larger.

Principal component regression on the hyperspectral image data yielded standard error of estimate (SEE) = 6.5 days, standard error of performance (SEP) = 6.7 days,  $r^2 = 0.86$ , RSD=12%, at  $p < 0.05$  using an F test for cross validation. A detection limit in days was calculated using the images and the PCR model ( $3 \times \text{SD}_{\text{blank}} = 3.3$  days). Of course, such a calibration should not really be linear, but instead a complex function of time, precipitation, and sunlight exposure. Environmental toxicology should also play a role in the refining the relationship between cyanobacteria and production of protectant molecules. The correlation between hyperspectral images and time was calculated in spite of the lack of a good reference assay for cyanobacteria in endolithic biofilms. Scanning electron microscopy (SEM) is often employed to study endolithic biofilms (Ascaso, 2002). However, stone contains microfissures and biofilms can penetrate on order of a few mm into the surface, making quantification difficult. These quantitative studies remain for future work. The dynamic range of the hyperspectral imaging technique must be defined for now in terms of time. The range extends from the detection limit given above to a maximum that is impossible to define because the camera can always be moved farther from the sample, at least in theory. The only limitation on distance between the camera and target for hyperspectral imaging appears to be the acceptable spatial resolution desired on the rock surface. The NASA near earth asteroid rendezvous spacecraft orbited the asteroid Eros in 2000 at a distance of 200 km, and successfully collected spectra from 804–2732 nm (Veverka, 2000). As the number of pixels on detector arrays increases, cameras can be located farther away and still maintain acceptable spatial resolution.

Possible interferences in hyperspectral imaging of endolithic biofilms include dirt accumulation on the surface. An interference test was conducted using indigenous pollen collected for the test. In the area where the tests were performed, hackberry pollen is often present at airborne concentrations of approximately 1000 grains/ $\text{m}^3$  or more in the spring months. A calibration was also calculated using a wafer surface dirtied with collected pollen. The results of PCR with hyperspectral images and time were SEE = 5.9 days, SEP=6.5 days,  $r^2 = 0.89$ , RSD = 12%,  $p < 0.05$  using an F test for cross validation. Given the pollen collection technique, other dust was also likely included. Nevertheless, no interference effect was noted in these results. The lack of effect is probably due to the multivariate calibration process, which

modeled the indigenous interferences and performed simultaneous multicomponent analyses of the analytes and interferences. Still, it seems likely that there might eventually be a small loss of sensitivity from dirt simply covering the surface physically. Other potential interferences that remain to be studied include different indigenous biofilms that might spread on the surface.

It has been suggested that scanning integration time should be constrained to one Mars day or less for a Mars mission. The potential problem with long hyperspectral image integrations that require sunlight to illuminate the rocks is that the reflectance angles change as the sun moves. If the measurement is made with a limited number of images of the rocks the measurement is more practical. Fortunately, the sensitivity of the camera systems usually permits images to be collected in far less than one day. On Earth, for example, the hyperspectral imaging systems aboard the Predator military reconnaissance aircraft are able to collect vast amounts of data in the visible and IR bands, and identify targets autonomously in real time on missions whose duration is far less than anticipated for a Martian mission (Naval Research Laboratory, 2000). In the future, application of wavelet theory to filter system design might enable more efficient imaging with fewer wavelength bands, speeding analysis or even resulting in better separation of the spectral groups at different time points.

Rocks could also be imaged for endolithic biofilms at night. The rover could station itself before sunset in a region that could be scanned in 360 degrees. The rover could use an array of solid-state IR or UV light sources to illuminate the rocks in the cameras' field of view. The rover could rotate in place, stopping as needed to acquire multiple IR, visible and UV images of the rocks. In this way, complete control of the wavelengths of light that illuminate the rocks is maintained, eliminating possible interference from sample fluorescence in reflectance measurements, and perhaps even enabling fluorescence images to be collected separately. In addition, the mission would not be constrained by having to pause for extended periods of time to image rocks when the rover should be driving. The rovers do not drive at night when there is no power available from the solar panels. There is usually sufficient battery power to rotate a rover in place and take images, however. The images could be stored in memory and processed in the morning when solar power is available.

## CONCLUSIONS

Scientists on Earth have focused their efforts in searches for extraterrestrial life onto robotic probes sent to nearby planets. Cyanobacteria are one of the oldest forms of life on Earth, and similar forms of life may have developed on other planets like Mars as well. The UV levels on earth vary slightly with elevation and ozone density, as well as with weather conditions. On planets such as Mars the UV radiation is much more intense. Future research will explore how the known strains of *Gloeocapsa* respond to UV levels comparable to those on Mars. The mechanisms by which the cyanobacteria adapt and the features that occur (e.g., higher absorbance, different spectra) will be defined. In contrast, organisms on moons in the solar system that are far away from the sun may actually have adapted to thrive on UV light rather than block it. A hyperspectral imaging system might also be used to find that kind of life. NASA has sent several missions to Mars intended to investigate the environment or to search for life, including the Mars Pathfinder / Sojourner mission. While the Pathfinder mission transmitted some of the best data obtained from the Martian surface to date, Sojourner had to drive up to a target to sample it. The search for life near locations where water may be intermittently present demands ability to sense life farther from the rover. The instrumentation must be durable and rugged for such a task. Cameras with tunable filters containing no moving parts are a step in the right direction in ruggedness. Hyperspectral imaging from a distance is able to easily monitor the distribution and spread of a cyanobacterium, *Gloeocapsa*, through spatial and spectrometric resolution of chemicals (MAAs and scytonemin) it produces to protect itself from UV radiation. The hyperspectral imaging system is flexible and can be calibrated to study the distribution of multiple analytes and interferences. A robotic rover with such an imaging system has the ability to drive up to the site and conduct more extensive sampling and collection because hyperspectral imaging is a nondestructive process.

## ACKNOWLEDGEMENTS

The authors thank the reviewers for contributing important suggestions for this paper. This paper made use of equipment and software obtained through NSF CHE-9257998 and DGE-9870691.

**LITERATURE CITED**

Ascaso, C. Wierzchos, J. Souza-Egipsy, V. de los Ríos A. and Delgado Rodrigues, J. In situ evaluation of the biodeteriorating action of microorganisms and the effects of biocides on carbonate rock of the Jeronimos Monastery, *International Biodeterioration & Biodegradation*, 49(1), 2002, 1-12.

Banerjee M; Whitton BA; Wynn-Williams DD, Phosphatase activities of endolithic communities in rocks of the Antarctic Dry Valleys. *Microbial Ecology.*, 39(1): 80-91, 2000

Naval Research Laboratory Press Release No. 60-00r, [http:// www.pao.nrl.navy.mil/rel-00/60-00r.html](http://www.pao.nrl.navy.mil/rel-00/60-00r.html), October 31 (2000)

Dempsey, R. J. Cassis, L.A. Davis, D.G. Lodder, R. A. "Near infrared imaging and spectroscopy in stroke research: Lipoprotein distributions and disease", *Ann. NY Acad. Sci.*, 820:149-169, 1997.

Garcia-Pichel, F., Wingard, C. E. and Castenholz, R. W. Evidence regarding the UV sunscreen role of a mycosporine-like compound in the cyanobacterium *Gloeocapsa* sp. *Appl. Environ. Microbiol.*, 59: 170-176, 1993a.

Garcia-Pichel, F and Castenholz, RW. Occurrence of UV-Absorbing, Mycosporine-Like Compounds among Cyanobacterial Isolates and an Estimate of Their Screening Capacity, *Appl. Environ. Microbiol.*, 59(1), 163-169, 1993b.

Malik, Imran; Poonacha, Mela; Moses, Jennifer and Lodder, Robert A. Multispectral Imaging of Tablets in Blister Packaging, *AAPS PharmSciTech* 2001; 2 (2) article 9 (<http://www.pharmscitech.com>).

Race, M. S., "Mars sample return and planetary protection in a public context." Meeting of the American Association for the Advancement of Science. Philadelphia, 1998.

Tough, A. The Internet As A Gateway To ETI. *Contact in Context* 2002, 1(1).

J. Veverka, M. Robinson, P. Thomas, S. Murchie, J. F. Bell III, N. Izenberg, C. Chapman, A. Harch, M. Bell, B. Carcich, A. Cheng, B. Clark, D. Domingue, D. Dunham, R. Farquhar, M. J. Gaffey, E. Hawkins, J. Joseph, R. Kirk,

H. Li, P. Lucey, M. Malin, P. Martin, L. McFadden, W. J. Merline, J. K. Miller, W. M. Owen Jr., C. Peterson, L. Prockter, J. Warren, D. Wellnitz, B. G. Williams, and D. K. Yeomans, "NEAR at Eros: Imaging and Spectral Results", *Science*, 2088- 2097, 22 Sept 2000.

Whitehouse, David "Martian water hunt leads to poles," BBCNews,SCI/TECH, [http://news.bbc.co.uk/1/hi/english/sci/tech/newsid\\_1410000/1410105.stm](http://news.bbc.co.uk/1/hi/english/sci/tech/newsid_1410000/1410105.stm), 27 June 200